Negative Kerr Nonlinearity of Graphene as seen via Chirped-Pulse-Pumped Self-Phase Modulation

Nathalie Vermeulen,[1,*] David Castelló-Lurbe,[1] JinLuo Cheng,[1,2] Iwona Pasternak,[3] Aleksandra Krajewska,[3] Tymoteusz Ciuk,[3] Wlodek Strupinski,[3] Hugo Thienpont,[1] and Jürgen Van Erps[1]

[1]*Brussels Photonics Team, Department of Applied Physics and Photonics, Vrije Universiteit Brussel, Pleinlaan 2, 1050 Brussel, Belgium*

[2]*Department of Physics, University of Toronto, 60 St. George Street, Toronto, Ontario M5S 1A7, Canada*

[3]*Institute of Electronic Materials Technology, Wolczynska 133, 01-919 Warsaw, Poland*

(Received 6 May 2016; revised manuscript received 3 September 2016; published 13 October 2016)

We experimentally demonstrate a negative Kerr nonlinearity for quasiundoped graphene. Hereto, we introduce the method of chirped-pulse-pumped self-phase modulation and apply it to graphene-covered silicon waveguides at telecom wavelengths. The extracted Kerr-nonlinear index for graphene equals $n_{2,\mathrm{gr}} = -10^{-13}$ m^2/W. Whereas the sign of $n_{2,\mathrm{gr}}$ turns out to be negative in contrast to what has been assumed so far, its magnitude is in correspondence with that observed in earlier experiments. Graphene's negative Kerr nonlinearity strongly impacts how graphene should be exploited for enhancing the nonlinear response of photonic (integrated) devices exhibiting a positive nonlinearity. It also opens up the possibility of using graphene to annihilate unwanted nonlinear effects in such devices, to develop unexplored approaches for establishing Kerr processes, and to extend the scope of the "periodic poling" method often used for second-order nonlinearities towards third-order Kerr processes. Because of the generic nature of the chirped-pulse-pumped self-phase modulation method, it will allow fully characterizing the Kerr nonlinearity of essentially any novel (2D) material.

DOI: 10.1103/PhysRevApplied.6.044006

I. INTRODUCTION

The emergence of graphene, a 2D honeycomb lattice of carbon atoms with a linear electronic band structure, has had an enormous impact on numerous research areas, including that of nonlinear optics. Already in 2010 Hendry and co-workers found the Kerr nonlinearity of graphene [1] to be extremely strong—a direct result from the material's unique band structure [2]—and this experimental observation attracted much attention from the broad community working on advanced Kerr-nonlinear light-generation phenomena such as supercontinuum and frequency-comb generation [3–5]. To extract graphene's Kerr nonlinearity, Hendry *et al.* use "free-space" laser excitation to establish four-wave mixing (FWM) in a graphene sample. Also free-space *Z*-scan measurements [6] are employed for this purpose. Meanwhile, the ever-increasing importance of integrated photonics encourages researchers to combine graphene's nonlinear optical properties with on-chip (semiconductor) waveguide structures [7–10]. Covering a waveguide with graphene dramatically changes the waveguide's nonlinear behavior because of the interaction between the evanescent tails of the guided mode and the 2D top layer. Despite graphene's very strong Kerr nonlinearity as was already demonstrated in 2010, a rather limited number of on-chip nonlinear-optical graphene devices have been reported on so far, and they mostly rely on FWM in graphene-covered silicon waveguides [7–10]. To pave the way to a more varied exploitation of graphene in nonlinear photonic integrated circuits and enable advanced nonlinear light generation, not only the strength or magnitude of graphene's Kerr nonlinearity has to be known, but also its sign needs to be measured, since the latter determines whether the nonlinear effects induced by the graphene and the underlying waveguide add or subtract. The Kerr coefficient of the graphene cover layer has been (tacitly) assumed to be positive in the demonstrated FWM devices, but in fact FWM intrinsically allows measuring only the coefficient's magnitude and not its sign. If with another method one can also assess the sign, this knowledge will enable researchers to fully exploit graphene's promise as an efficiency-enhancing material in essentially any nonlinear photonic system. In this article, we examine both the magnitude and the sign of graphene's Kerr nonlinearity using a different approach, namely, by means of chirped-pulse-pumped self-phase modulation (SPM) experiments in graphene-covered silicon waveguides.

II. BASIC PRINCIPLES OF CHIRPED-PULSE-PUMPED SPM

The following explanation on the physics of the chirped-pulse-pumped SPM approach shows that, as opposed to FWM experiments, it does enable assessing the sign of a

*Corresponding author.
nvermeul@b-phot.org

material's Kerr nonlinearity. SPM is a Kerr process that broadens or narrows the spectral width of an input laser pulse [11,12]. This broadening or narrowing effect can become very pronounced even at modest excitation powers, provided that the input pulse exhibits chirp. Let us consider a waveguide section of length Δz in which a pulse propagates with amplitude $A(z,t) = |A(z,t)|\exp[i\varphi(z,t)]$. For a Fourier-transformed amplitude $\tilde{A}(z,\omega-\omega_0)$ centered at frequency ω_0, the square of the rms spectral width can be written as $\mu_2(z) = [\int_{-\infty}^{\infty}(\omega-\omega_0)^2|\tilde{A}(\omega-\omega_0)|^2 d\omega]/[\int_{-\infty}^{\infty}|\tilde{A}(\omega-\omega_0)|^2 d\omega]$ [12,13], which in the time domain can be expressed as $\mu_2(z) = (\int_{-\infty}^{\infty}|\partial_t A|^2 dt)/(\int_{-\infty}^{\infty}|A|^2 dt)$ [12]. For the experiments reported in this paper, the pulse propagation is mostly determined by Kerr-nonlinear effects rather than dispersion and free-carrier effects (which is also verified numerically with the inclusion of graphene-generated free carriers [13,14]). Hence, we can adopt a simplified version of the nonlinear Schrödinger equation incorporating only SPM effects and linear loss: $\partial_z A = -(\alpha/2)A + i\gamma_K|A|^2 A$, with γ_K the Kerr nonlinearity and α the linear loss coefficient. This yields

$$|A(\Delta z,t)|^2 = \exp[-\alpha\Delta z]|A(0,t)|^2,$$
$$\varphi(\Delta z,t) = \varphi(0,t) + \gamma_K|A(0,t)|^2\Delta z_{\text{eff}}, \tag{1}$$

where $\Delta z_{\text{eff}} = [1-\exp(-\alpha\Delta z)]/\alpha$ represents the effective length. When rewriting $A(0,t)$ as $A(0,t) = \sqrt{P_0}U_0(t)\exp[i\varphi_0(t)]$ with P_0 the input peak power, implementing Eq. (1) in $\mu_2(z)$ results in the following expression for the relative spectral broadening factor $\mu_2(\Delta z)/\mu_2(0)$ after propagation over Δz:

$$\frac{\mu_2(\Delta z)}{\mu_2(0)} = 1 + \frac{2\gamma_K P_0\Delta z_{\text{eff}}\sigma_3/\sigma_1 + (\gamma_K P_0\Delta z_{\text{eff}})^2\sigma_4/\sigma_1}{1+\sigma_2/\sigma_1} \tag{2}$$

with $\sigma_{1,2,3,4}$ being the input pulse shape factors:

$$\sigma_1 = \frac{\int_{-\infty}^{\infty}(\partial_t U_0)^2 dt}{\int_{-\infty}^{\infty}U_0^2 dt}, \qquad \sigma_2 = \frac{\int_{-\infty}^{\infty}(\partial_t\varphi_0)^2 U_0^2 dt}{\int_{-\infty}^{\infty}U_0^2 dt},$$
$$\sigma_3 = \frac{\int_{-\infty}^{\infty}(\partial_t\varphi_0)(\partial_t U_0^2)U_0^2 dt}{\int_{-\infty}^{\infty}U_0^2 dt}, \qquad \sigma_4 = \frac{\int_{-\infty}^{\infty}(\partial_t U_0^2)^2 U_0^2 dt}{\int_{-\infty}^{\infty}U_0^2 dt}. \tag{3}$$

When assuming a quadratic input phase profile $\varphi(0,t) = -C_0 t^2/T_0^2$ with input chirp parameter C_0, Eq. (2) yields

$$\frac{\mu_2(\Delta z)}{\mu_2(0)} = 1 + \frac{2\gamma_K P_0\Delta z_{\text{eff}}C_0\sigma_{31} + (\gamma_K P_0\Delta z_{\text{eff}})^2\sigma_{41}}{1+4C_0^2\sigma_{21}} \tag{4}$$

with the new dimensionless shape factors $\sigma_{21,31,41}$ all having positive values determined by

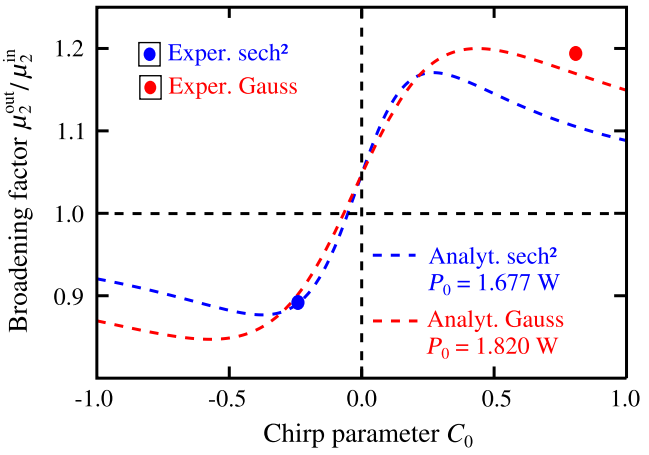

FIG. 1. Illustration of the broadening factor dependence on the input chirp parameter for a silicon waveguide and for Gaussian and sech^2 input pulses as used in our experiments.

$$\sigma_{21} = \frac{1}{T_0^4}\frac{\int_{-\infty}^{\infty}t^2U_0^2 dt}{\int_{-\infty}^{\infty}(\partial_t U_0)^2 dt}, \qquad \sigma_{31} = \frac{1}{T_0^2}\frac{\int_{-\infty}^{\infty}U_0^4 dt}{\int_{-\infty}^{\infty}(\partial_t U_0)^2 dt},$$
$$\sigma_{41} = \frac{\int_{-\infty}^{\infty}(\partial_t U_0^2)^2 U_0^2 dt}{\int_{-\infty}^{\infty}(\partial_t U_0)^2 dt}. \tag{5}$$

For a Gaussian pulse with $U_0^2 = \exp(-t^2/T_0^2)$ and a sech^2 pulse with $U_0^2 = \text{sech}^2(t/T_0)$, these shape factors become, respectively, $\sigma_{21} = 1$ and $\pi^2/4$; $\sigma_{31} = \sqrt{2}$ and 2; and $\sigma_{41} = 4/(3\sqrt{3})$ and $32/35$. We point out that for $C_0 = 0$ only the term containing σ_{41} remains, and the formula reported in Ref. [12] is recovered.

Equation (4), in fact, corresponds to earlier-presented SPM formulas [11,12] while also taking into account the input chirp parameter. In the high-power regime, the term proportional to $(\gamma_K P_0\Delta z_{\text{eff}})^2$ in Eq. (4) will be dominant, and the broadening factor will be larger than 1 with the highest value attained at $C_0 = 0$, i.e., for a transform-limited input pulse [15]. At low powers, however, the term proportional to $2\gamma_K P_0\Delta z_{\text{eff}}C_0$ becomes important, and, depending on the sign of $\gamma_K C_0$ [16], the broadening factor can be either larger or smaller than 1 (i.e., one has either broadening or narrowing), with a maximum or minimum value at a nonzero chirp C_0. As such, when exciting a waveguide with a low-power pulse exhibiting an appropriately chosen chirp C_0, the nature of the spectral width modification, i.e., broadening or narrowing, will indicate the sign of the waveguide's Kerr nonlinearity γ_K. This is also illustrated in Fig. 1, depicting the spectral broadening factor of Eq. (4) as a function of C_0 for a silicon waveguide (see further on), the Kerr nonlinearity of which is known to be positive at wavelengths above 1000 nm [17]. In Fig. 1, the spectral broadening and narrowing obtained at, respectively, substantially positive and negative C_0 values indeed unambiguously demonstrate the positive sign of silicon's Kerr nonlinearity [18]. In a similar way, by

carrying out chirped-pulse-pumped SPM experiments with graphene-covered silicon waveguides and factoring out silicon's nonlinear response, we can determine the sign of graphene's Kerr nonlinearity.

III. EXPERIMENTAL SETUP AND RESULTS

To perform such chirped-pulse-pumped SPM experiments, we employ grating-coupled bare and graphene-covered silicon-on-insulator (SOI) waveguide structures designed for operation around the 1550-nm telecom wavelength and all featuring the same layout for the gratings, tapers, and the actual waveguide section [see Fig. 2(a)]. The waveguide's cross section has a width of 450 nm and a height of 220 nm, which is standard for SOI chips fabricated by ePIXfab [19]. Because of the identical layouts of the bare and graphene-covered SOI waveguides, the bare waveguide can serve as a reference structure with a well-known Kerr nonlinearity magnitude and sign at 1550 nm. We also consider this waveguide for plotting the theoretical broadening factor in Fig. 1, where we apply the model of Eq. (4) to the taper and waveguide sections in a cascaded way. Hereto, we use $\alpha_{\mathrm{SOI}} = 3$ dB/cm and $\gamma_{\mathrm{SOI}} = +0.3$ W^{-1} mm^{-1} [13] in the waveguide section, and we assume a scaling of these parameters inversely proportional with the waveguide width in the tapered sections. The graphene deposition on the waveguides has been described in our earlier work [20]. Chemical-vapor-deposition-grown graphene is transferred on the SOI chip, inducing a high linear waveguide loss of $\alpha_{\mathrm{gr\text{-}on\text{-}SOI}} = 1320$ dB/cm at 1550 nm, and the layer is patterned to vary the length of the graphene sections on top of the waveguides [20]. The Fermi energy of the graphene sheet is about −0.2 eV as a result of weak unintentional doping induced by the transfer process itself [21], so that at 1550 nm we are operating in graphene's high-loss regime above its single-photon absorption threshold.

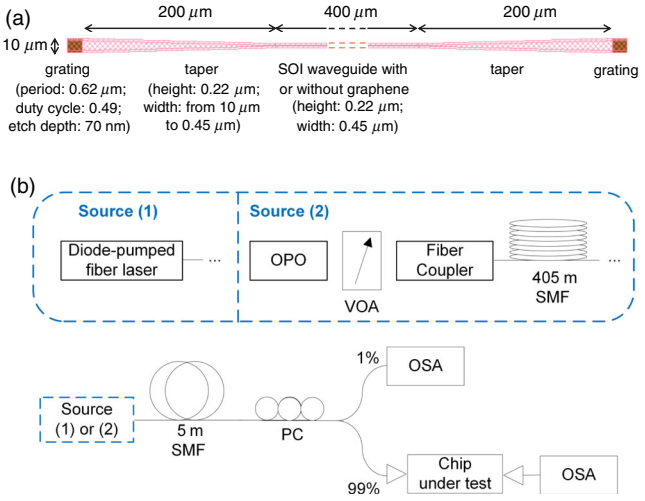

FIG. 2. (a) Outline of the employed waveguide structures. (b) Experimental setup for the SPM measurements.

We carry out SPM measurements for both a positive and negative input chirp using the experimental setup shown in Fig. 2(b). The pulsed-laser sources used to excite the waveguides are a diode-pumped fiber laser [Calmar FPL-02CTF-POL; source (1) in Fig. 2(b)] and a fiber-coupled optical parametric oscillator (OPO) [APE Levante IR with a variable optical attenuator (VOA); source (2)] generating, respectively, Gaussian pulses at a repetition rate of 40 MHz and sech^2 pulses at a repetition rate of 80 MHz. The pulses are coupled into and out of the waveguides by means of flat-cleaved fiber probes positioned above the waveguides' grating couplers at an angle of 9° with respect to the vertical axis. We ensure the excitation of the transverse-electric (TE) mode in the waveguides using a fiber-based polarization controller (PC). To monitor the input spectrum, a 99:1 coupler is inserted in the setup to split off 1% of the laser power towards a fiber-coupled optical spectrum analyzer (OSA) [Yokogawa AQ6370D] just in front of the incoupling fiber probe. Simultaneously with the input spectrum, the output spectrum is measured with a second fiber-coupled optical spectrum analyzer just behind the outcoupling fiber probe. Prior to the SPM measurements, we measure the pulses' temporal characteristics by means of a frequency-resolved optical gating (FROG) instrument [Coherent Solutions HR150]. The actual SPM measurements consist of simultaneously recording the rms spectral widths of the input and output spectra for the waveguides with graphene lengths varying from 0 to 250 μm in steps of 50 μm.

For the experiments with a positive input chirp, we employ the diode-pumped fiber laser set at an operation wavelength of 1550 nm, with the laser pulses guided over 5 m of G.652 single-mode fiber (SMF) towards the waveguides. The measured temporal power and phase profiles as shown in Fig. 3 yield a full-width-at-half-maximum pulse length $T_{\mathrm{FWHM},0} = 1.2$ ps and a fitted chirp parameter $C_0 = 0.8$. The latter is extracted from the quadratically fitted phase profile indicated as the dotted green line

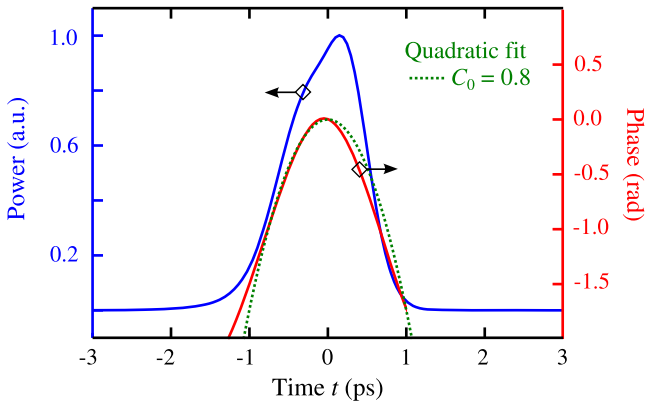

FIG. 3. FROG-measured temporal power profile (solid blue line) and phase profile (solid red line) of the input pulses with positive chirp. The dotted green line is the quadratically fitted phase.

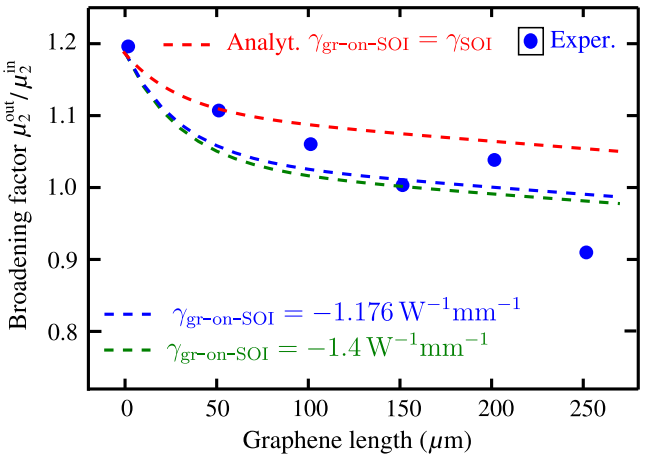

FIG. 4. Broadening factor vs graphene length for a positive input chirp. The analytical dashed curves serve for fitting.

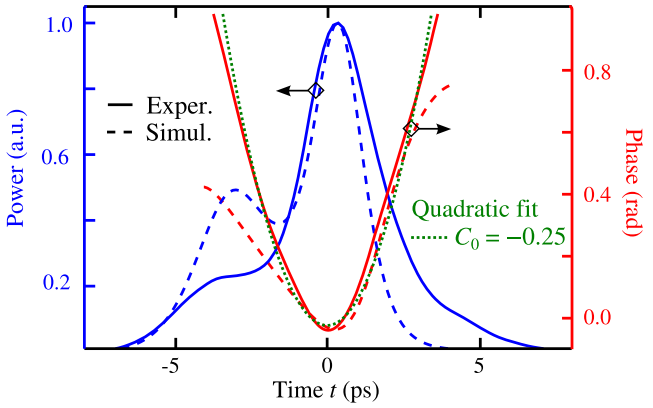

FIG. 5. FROG-measured (solid lines) and numerically simulated (dashed lines) temporal power profile (blue) and phase profile (red) of the input pulses with negative chirp. The dotted green line is the quadratically fitted phase.

in Fig. 3. The peak power coupled into the waveguide is set at 1.82 W. The measured broadening factors as a function of the graphene length on top of the waveguides are depicted in Fig. 4. Since the input pulses are positively chirped, we observe for the bare SOI waveguide (graphene length of 0 μm) with $\gamma_{\text{SOI}} > 0$ spectral broadening as expected. The measured broadening factor lies close to the corresponding theoretical value at $C_0 = 0.8$ in Fig. 1. The latter shows that the simple theory of Eq. (4) without the inclusion of two-photon absorption or free-carrier effects is an adequate model for our experiments with modest peak powers, relatively short pulse durations, and short waveguide lengths. For the SOI waveguides covered with graphene, the level of spectral broadening is reduced with increasing graphene length, and for sufficiently long graphene sections even spectral narrowing is observed. We point out that, since the graphene cover layers are situated in the center of the 400-μm-long waveguide sections [20], all waveguides have an uncovered SOI section at the input with $\gamma_{\text{SOI}} > 0$ establishing spectral broadening. As shown in Fig. 4, this broadening is progressively counteracted by the graphene-covered sections, which consequently feature $\gamma_{\text{gr-on-SOI}} < 0$. This observation also showcases that depositing graphene on another nonlinear material will not always enhance the nonlinear response of the material system and in some cases even annihilates its nonlinear behavior.

The latter finding is also confirmed in our experiments with a negative input chirp. Hereto, we employ the OPO source tuned to a wavelength of 1553 nm. The pulses at the free-space output of the OPO are slightly positively chirped, but, when coupled into a G.652 fiber with an appropriately chosen length, a negative pulse chirp can be obtained at the output of the fiber. Indeed, during propagation in the fiber, the pulses initially experience spectral broadening due to SPM effects in the fiber. At the same time, they are compressed in time due to the negative group-velocity dispersion ($\beta_2 < 0$) of the G.652 single-mode fiber in the telecom window around 1550 nm. As such, after having traveled a certain propagation distance, the pulses become transform limited ($C = 0$), and, beyond this point, they acquire a negative chirp induced by the fiber's negative β_2 [11]. Based on numerical simulations, we find that 6-ps-long OPO pulses with a peak power of 12 W at the fiber input would reach this regime of negative chirp at a propagation distance of around 410 m. Figure 5 shows both the measured and numerically simulated temporal power and phase profiles at the output of a 410-m-long fiber, as well as the quadratic fit of the experimental phase. The pulse length and chirp parameter are found to be $T_{\text{FWHM},0} = 3$ ps and $C_0 = -0.25$, respectively. The peak power coupled into the chip is set at 1.677 W. Figure 6 shows the measured broadening factors as a function of the graphene length on top of the waveguides. In view of the negative input chirp, we observe for the bare waveguide with $\gamma_{\text{SOI}} > 0$ spectral narrowing, with again a very good match between the measured spectral narrowing and the corresponding theoretical value at $C_0 = -0.25$ in Fig. 1. For the waveguides

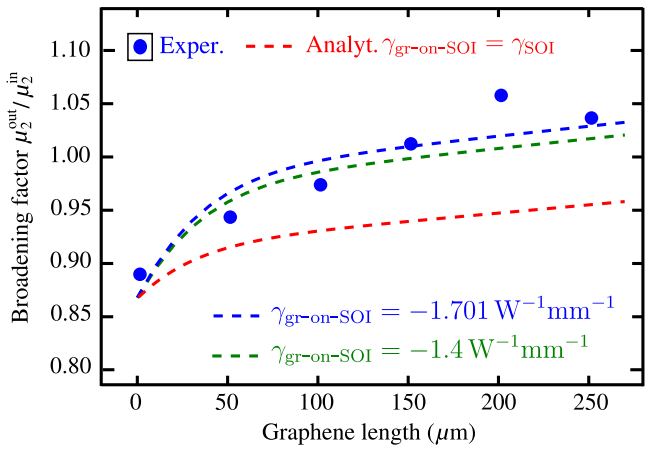

FIG. 6. Broadening factor vs graphene length for a negative input chirp. The analytical dashed curves serve for fitting.

with graphene on top, we find that this narrowing is progressively counteracted by the graphene-covered sections exhibiting $\gamma_{\text{gr-on-SOI}} < 0$.

Besides extracting the sign of $\gamma_{\text{gr-on-SOI}}$ in the graphene-covered waveguide sections, we also evaluate its magnitude by fitting our model with the data points of Figs. 4 and 6 while using only $\gamma_{\text{gr-on-SOI}}$ as a fitting parameter. In this case, we use the more generalized model of Eq. (2) rather than Eq. (4) and again apply it to both the taper and waveguide sections in a cascaded way. Optimal fitting is achieved by minimizing the fitting error $\sigma = \sqrt{(1/N)\sum_{i=1}^{N}(x_i - y_i)^2}$ with N the number of data points and with x_i and y_i the experimental and theoretical broadening factors, respectively. For Figs. 4 and 6, the optimal fitting is obtained for two very large, yet different nonlinearity values: $\gamma_{\text{gr-on-SOI}} = -1.176\ \text{W}^{-1}\,\text{mm}^{-1}$ yielding $\sigma_{\text{min}} = 0.043$ and $\gamma_{\text{gr-on-SOI}} = -1.701\ \text{W}^{-1}\,\text{mm}^{-1}$ yielding $\sigma_{\text{min}} = 0.022$, respectively. However, their average $-1.4(\pm 0.4)\ \text{W}^{-1}\,\text{mm}^{-1}$ [22] yields an equally high-quality fitting of the experimental data. Indeed, using $\gamma_{\text{gr-on-SOI}} = -1.4\ \text{W}^{-1}\,\text{mm}^{-1}$ results in approximately the same fitting error as when employing the two different nonlinearity values ($\sigma = 0.044$ vs 0.043 for Fig. 4 and $\sigma = 0.024$ vs 0.022 for Fig. 6) [23]. In contrast, a poor fitting is obtained when assuming the graphene-covered waveguide sections to exhibit the same nonlinearity as the bare waveguide (i.e., $\gamma_{\text{gr-on-SOI}} = \gamma_{\text{SOI}}$), which showcases the strong nonlinear impact of the graphene cover layer.

IV. EXTRACTING THE KERR NONLINEARITY OF GRAPHENE

From the value $-1.4\ \text{W}^{-1}\,\text{mm}^{-1}$ obtained for the *effective* Kerr nonlinearity $\gamma_{\text{gr-on-SOI}}$ in the graphene-covered waveguide sections, we can extract the nonlinearity of the graphene sheet itself using our earlier-presented weighted-contributions formalism for hybrid waveguides [14]. Starting from the actual waveguide mode profile in the presence of the graphene top layer and the corresponding propagation characteristics, this formalism, included in the Appendix, calculates the weighted nonlinearity contributions of the graphene cover layer and of the underlying silicon material to the effective nonlinearity $\gamma_{\text{gr-on-SOI}}$. Since $\gamma_{\text{gr-on-SOI}}$ is the parameter that we derive from the experiments, and since we can readily calculate the weighted nonlinearity contribution of the silicon waveguide, the formula in the Appendix allows extracting the nonlinearity of the graphene layer itself. This is done in two steps: First, from the formula we derive that, as most of the modal power resides in the silicon material, the contribution of the silicon to $\gamma_{\text{gr-on-SOI}} = -1.4\ \text{W}^{-1}\ \text{mm}^{-1}$ is given by γ_{SOI} of the bare waveguide, and that of the graphene cover layer equals $(-1.4\text{–}0.3) = -1.7\ \text{W}^{-1}\,\text{mm}^{-1}$. Second, by assessing specifically the expression for the graphene contribution (i.e., the second term in the formula in the Appendix), we then extract that the graphene sheet as an isolated material features a Kerr-nonlinear index $n_{2,\text{gr}}$ of about $-10^{-13}\ \text{m}^2/\text{W}$ or a susceptibility $\chi^{(3)}_{\text{gr}}$ around -10^{-7} esu. Its magnitude is in line with earlier-reported graphene nonlinearity values [2,7], but the negative sign is not accounted for in those experiments. We point out that our earlier-presented calculations for the Kerr nonlinearity of graphene [24–26], although underestimating its absolute value, do predict a negative sign for the nonlinearity of quasiundoped graphene at optical wavelengths, both in the ideal case of zero electron scattering and in the case of considerable inter- and intraband scattering. The calculations show a negative Kerr nonlinearity resonance at the single-photon absorption threshold, and the negative nonlinearity sign persists also far above this threshold.

V. CONCLUSION

In conclusion, using the chirped-pulse-pumped SPM method introduced here—a generic method that allows extracting both the magnitude and the sign of the Kerr nonlinearity of any novel (2D) material [27]—we demonstrate a negative Kerr nonlinearity for quasiundoped graphene, whereas the magnitude of the obtained value is in line with earlier experimental reports. Our findings imply that, when using graphene to enhance the nonlinear response of a photonic device or integrated circuit with a positive nonlinearity, one needs to carefully study how the 2D material should be implemented to actually achieve a net enhancement. Our results also show that, when targeting the compensation of unwanted nonlinearities in such a device or circuit, graphene could be of use as well. Finally, graphene's negative Kerr nonlinearity can open up unexplored approaches for establishing Kerr interactions and even extend the scope of, e.g., the "periodic poling" method often used for second-order nonlinearities [28] towards third-order Kerr processes.

ACKNOWLEDGMENTS

This work is supported by the ERC-FP7/2007-2013 Grant No. 336940, the EU-FET GRAPHENICS Project No. 618086, the Hercules-stichting Grant No. UABR/007/09, the FWO Project No. G.A002.13N, the EU-FP7 Graphene Flagship 604391, VUB-OZR, BELSPO-IAP, and Methusalem.

APPENDIX: WEIGHTED-CONTRIBUTIONS FORMALISM

Below, we briefly summarize the basic concepts of the weighted-contributions formalism used for extracting the graphene nonlinearity from the measured effective nonlinearity; for further details about this formalism, we refer to Ref. [14]. When assuming a graphene-covered silicon waveguide oriented along the ζ direction, we can write the electric field associated with a waveguide mode as proportional to $\mathbf{e}_\mu(x,y)e^{ik_\mu\zeta}$, where $\mu = p$ indicates the mode profile excited by the pump laser used; we assume the

normal to the top of the waveguide to be $\hat{\mathbf{y}}$. When determining this modal field using mode-solver software, we incorporate the linear optical properties of silicon (assumed lossless at the wavelength of interest) and treat the graphene layer as a thin sheet with thickness d_{gr} on top of the waveguide. We employ the function $s_{\mathrm{Si}}(x,y)$ [$s_{\mathrm{gr}}(x,y)$] to indicate where the silicon [graphene] is situated; $s_{\mathrm{Si}}(x,y)=1$ [$s_{\mathrm{gr}}(x,y)=1$] where the silicon [the thin layer modeling the graphene] is present, and $s_{\mathrm{Si}}(x,y)=0$ [$s_{\mathrm{gr}}(x,y)=0$] where the silicon [the thin layer modeling the graphene] is absent. We obtain the following formula for the effective Kerr nonlinearity measured in the self-phase modulation experiments with the graphene-covered silicon waveguides:

$$\begin{aligned}\gamma_{\text{gr-on-SOI}} &= \gamma_{\text{SOI,weighted}} + \gamma_{\text{gr,weighted}} \\ &= (4v_p^2 I_p^2)^{-1} 3\epsilon_0 \omega_p \chi_{\mathrm{Si}}^{(3),ijkl} \int [e_p^i(x',y')]^* e_p^j(x',y')[e_p^k(x',y')]^* e_p^l(x',y') s_{\mathrm{Si}}(x',y')dx'dy' \\ &\quad + (4v_p^2 d_{\mathrm{gr}} I_p^2)^{-1} 3i\sigma_{\mathrm{gr}}^{(3),ijkl} \int [e_p^i(x',y')]^* e_p^j(x',y')[e_p^k(x',y')]^* e_p^l(x',y') s_{\mathrm{gr}}(x',y')dx'dy', \end{aligned} \tag{A1}$$

with $\gamma_{\text{SOI,weighted}}$ and $\gamma_{\text{gr,weighted}}$ the weighted nonlinearity contributions from the underlying SOI waveguide and the graphene top layer, respectively. v_p and I_p are scaling factors defined in Ref. [14], ϵ_0 is the dielectric permittivity, ω_p is the pump frequency, $\chi_{\mathrm{Si}}^{(3),ijkl}$ represents the third-order Kerr-nonlinear susceptibility of silicon, and $\sigma_{\mathrm{gr}}^{(3),ijkl}$ is the third-order Kerr-nonlinear conductivity of graphene. The latter can be converted to a susceptibility using $\chi=\sigma/(-i\omega\epsilon_0 d_{gr})$ [24].

[1] We here refer to the parametric Kerr effect, which differs from the nonparametric saturable absorption effect in graphene.

[2] E. Hendry, P. J. Hale, J. Moger, A. K. Savchenko, and S. A. Mikhailov, Coherent Nonlinear Optical Response of Graphene, Phys. Rev. Lett. **105**, 097401 (2010).

[3] R. Holzwarth, T. Udem, T. W. Hansch, J. C. Knight, W. J. Wadsworth, and P. S. J. Russell, Optical Frequency Synthesizer for Precision Spectroscopy, Phys. Rev. Lett. **85**, 2264 (2000).

[4] T. J. Kippenberg, R. Holzwarth, and S. A. Diddams, Microresonator-based optical frequency combs, Science **332**, 555 (2011).

[5] N. Savage, Supercontinuum sources, Nat. Photonics **3**, 114 (2009).

[6] H. Zhang, S. Virally, Q. Bao, L. K. Ping, S. Massar, N. Godbout, and P. Kockaert, Z-scan measurement of the nonlinear refractive index of graphene, Opt. Lett. **37**, 1856 (2012).

[7] T. Gu, N. Petrone, J. F. McMillan, A. van der Zande, M. Yu, G. Q. Lo, D. L. Kwong, J. Hone, and C. W. Wong, Regenerative oscillation and four-wave mixing in graphene optoelectronics, Nat. Photonics **6**, 554 (2012).

[8] H. Zhou, T. Gu, J. F. McMillan, N. Petrone, A. van der Zande, J. C. Hone, M. Yu, G. Lo, D.-L. Kwong, G. Feng, S. Zhou, and C. W. Wong, Enhanced four-wave mixing in graphene-silicon slow-light photonic crystal waveguides, Appl. Phys. Lett. **105**, 091111 (2014).

[9] M. Ji, H. Cai, L. Deng, Y. Huang, Q. Huang, J. Xia, Z. Li, J. Yu, and Y. Wang, Enhanced parametric frequency conversion in a compact silicon-graphene microring resonator, Opt. Express **23**, 18679 (2015).

[10] X. Hu, Y. Long, M. Ji, A. Wang, L. Zhu, Z. Ruan, Y. Wang, and J. Wang, Graphene-silicon microring resonator enhanced all-optical up and down wavelength conversion of QPSK signal, Opt. Express **24**, 7168 (2016).

[11] G. P. Agrawal, *Nonlinear Fiber Optics*, 4th ed. (Academic, New York, 2007).

[12] S. C. Pinault and M. J. Potasek, Frequency broadening by self-phase modulation in optical fibers, J. Opt. Soc. Am. B **2**, 1318 (1985).

[13] D. Castelló-Lurbe and E. Silvestre, Supercontinuum generation in silicon waveguides relying on wave-breaking, Opt. Express **23**, 25462 (2015).

[14] N. Vermeulen, J. L. Cheng, J. E. Sipe, and H. Thienpont, Opportunities for wideband wavelength conversion in foundry-compatible silicon waveguides covered with graphene, IEEE J. Sel. Top. Quantum Electron. **22**, 8100113 (2016).

[15] O. Boyraz, T. Indukuri, and B. Jalali, Self-phase-modulation induced spectral broadening in silicon waveguides, Opt. Express **12**, 829 (2004).

[16] We point out that for *temporal* pulse broadening or narrowing in a waveguide with dispersion β_2, the sign of $\beta_2 C_0$ plays an analogous role [11].

[17] A. D. Bristow, N. Rotenberg, and H. M. van Driel, Two-photon absorption and Kerr coefficients of silicon for 850–2200 nm, Appl. Phys. Lett. **90**, 191104 (2007).

[18] In the low-power regime, spectral broadening can also be obtained at a negative input chirp (see center region of Fig. 1), provided that the chirp value is sufficiently close to zero to let the last term in Eq. (4) dominate.

[19] http://www.epixfab.eu/.

[20] J. Van Erps, T. Ciuk, I. Pasternak, A. Krajewska, W. Strupinski, S. Van Put, G. Van Steenberge, K. Baert, H. Terryn, H. Thienpont, and N. Vermeulen, Laser ablation- and plasma etching-based patterning of graphene on silicon-on-insulator waveguides, Opt. Express **23**, 26639 (2015).

[21] T. Ciuk, I. Pasternak, A. Krajewska, J. Sobieski, P. Caban, J. Szmidt, and W. Strupinski, Properties of chemical vapor

deposition graphene transferred by high-speed electrochemical delamination, J. Phys. Chem. C **117**, 20833 (2013).

[22] The tolerance interval is calculated using the same formula as for the fitting error σ but with x_i the two optimum fitting values and y_i their average.

[23] Also when measuring the broadening factor as a function of input peak power instead of graphene length, we extract the same value for $\gamma_{\text{gr-on-SOI}}$.

[24] J. L. Cheng, N. Vermeulen, and J. E. Sipe, Third order optical nonlinearity of graphene, New J. Phys. **16**, 053014 (2014).

[25] J. L. Cheng, N. Vermeulen, and J. E. Sipe, Third-order nonlinearity of graphene: Effects of phenomenological relaxation and finite temperature, Phys. Rev. B **91**, 235320 (2015).

[26] J. L. Cheng, N. Vermeulen, and J. E. Sipe, Numerical study of the optical nonlinearity of doped and gapped graphene: From weak to strong field excitation, Phys. Rev. B **92**, 235307 (2015).

[27] A. Castellanos-Gomez, Why all the fuss about 2D semiconductors?, Nat. Photonics **10**, 202 (2016).

[28] D. S. Hum and M. M. Fejer, Quasi-phasematching, C.R. Phys. **8**, 180 (2007).